Hearing Research 309 (2014) 63–74

Contents lists available at ScienceDirect

Hearing Research

journal homepage: www.elsevier.com/locate/heares

Research paper

Vestibular receptors contribute to cortical auditory evoked potentials

Neil P.M. Todd [a,*], Aurore C. Paillard [a], Karolina Kluk [a], Elizabeth Whittle [a], James G. Colebatch [b]

[a] The University of Manchester, UK
[b] University of New South Wales, Australia

ARTICLE INFO

Article history:
Received 13 August 2013
Received in revised form
8 October 2013
Accepted 26 November 2013
Available online 7 December 2013

ABSTRACT

Acoustic sensitivity of the vestibular apparatus is well-established, but the contribution of vestibular receptors to the late auditory evoked potentials of cortical origin is unknown. Evoked potentials from 500 Hz tone pips were recorded using 70 channel EEG at several intensities below and above the vestibular acoustic threshold, as determined by vestibular evoked myogenic potentials (VEMPs). In healthy subjects both auditory mid- and long-latency auditory evoked potentials (AEPs), consisting of Na, Pa, N1 and P2 waves, were observed in the sub-threshold conditions. However, in passing through the vestibular threshold, systematic changes were observed in the morphology of the potentials and in the intensity dependence of their amplitude and latency. These changes were absent in a patient without functioning vestibular receptors. In particular, for the healthy subjects there was a fronto-central negativity, which appeared at about 42 ms, referred to as an N42, prior to the AEP N1. Source analysis of both the N42 and N1 indicated involvement of cingulate cortex, as well as bilateral superior temporal cortex. Our findings are best explained by vestibular receptors contributing to what were hitherto considered as purely auditory evoked potentials and in addition tentatively identify a new component that appears to be primarily of vestibular origin.

1. Introduction

In many fish and amphibian species the otolith organs (the saccule and utricle) are important for the detection of sound, as well as serving a vestibular function (Lewis and Narins, 1999). Throughout vertebrate evolution, new structures evolved for the detection of sound culminating in the cochlea (Manley et al., 2004). Nevertheless, an acoustic sensitivity of the otolith organs has been conserved in all classes of vertebrate, including primates (Young et al., 1977; McCue and Guinan, 1994; Curthoys et al., 2006). In humans, acoustic sensitivity of the otolith organs can be demonstrated by vestibular-dependent effects like nystagmus (Lackner and Graybiel, 1974) or evoked electromyographic (EMG) signals (Bickford et al., 1964). Such EMG responses can be measured either from muscles of the neck, e.g. the sternocleidomastoid muscle, reflecting the vestibular-collic reflex pathways (the vestibular evoked myogenic potential or VEMP: Colebatch et al., 1994) or from extra-ocular eye muscles, reflecting activation of the vestibular ocular reflex pathways (ocular VEMP or OVEMP: Rosengren et al., 2005; Todd et al., 2007). Although the neck response is often now referred to as a cervical VEMP (or CVEMP), in the rest of this text we use the original acronym VEMP.

The use of vestibular evoked EMG methods has enabled considerable advances in our knowledge of the sensitivity of the human otolith organs to acoustic stimulation. Within the literature there is, however, considerable confusion in the use of terms, especially with the introduction of the mini-shaker (e.g. model 4810, Bruel & Kjaer, Denmark) as a means of stimulation, along with the usual head-phones for the delivery of air-conducted (AC) sound, and the more conventional audiological vibrator (e.g. model B71, Radioear Corp., USA) for bone-conducted (BC) sound. The principal source of confusion is that the nature of the skull response changes as a function of stimulus frequency. At the higher frequencies typically employed in audiometry, the skull response is primarily a function of its reactive, i.e. elastic, properties, but for low-frequencies, less than about 800–1000 Hz, the skull response is characterised as whole-head quasi-rigid vibration in which there is zero phase between stimulus and response (Stenfelt et al., 2000; McKnight et al., 2013). This is further complicated by the existence of several skull resonances near 500 Hz. In order to

* Corresponding author. Faculty of Life Science, University of Manchester, Manchester M13 9PL, UK. Tel.: +44(0)161 306 5770.
E-mail address: neil.todd@manchester.ac.uk (N.P.M. Todd).

0378-5955
http://dx.doi.org/10.1016/j.heares.2013.11.008

distinguish these response regimes we use here the terms BC sound vs. low-frequency vibration, with the transition placed at around 200 Hz, just below the skull resonances.

In response to sound and vibration the two otolith organs appear to have distinct tuning properties, with the saccule and utricle tuned to approximately 500 Hz and 100 Hz respectively (Todd and Cody, 2000; Todd et al., 2009), likely a consequence of underlying biomechanical properties. Recently, Zhang et al. (2011, 2012) showed that stimulation with both head-phones and mini-shaker may produce distinct resonances at about 100 Hz and 500 Hz, suggesting that the two resonance peaks are specific to the different dynamic responses of the two end-organs. Sound and vibration modes of stimulation also have distinct threshold properties. For 500 Hz AC sound activation, vestibular thresholds are found at about 80 dB above the auditory thresholds (Todd et al., 2008b), while using 100 Hz vibration, vestibular thresholds may be as low as 15 dB *below* the auditory threshold (Todd et al., 2008a).

Having made some progress in establishing the natural frequencies and appropriate modes of stimulation of the otolith organs, these sensitivities may be used as a tool to investigate the central pathways, i.e. by stimulating at best frequency for the receptors one is maximally likely to excite higher order neurons. Several attempts have now been made to measure vestibular evoked potentials (VsEPs) of neurogenic origin. Following a study by de Waele et al. (2001), which showed the existence of short-latency potentials (8–15 ms) in response to electrical stimulation, Todd et al. (2003) demonstrated a similar response to 500 Hz BC sound. These acoustically evoked short-latency VsEPs were confirmed as being vestibular as they were absent in avestibular patients but present in deaf subjects with intact VEMPs (Rosengren and Colebatch, 2006). A later study by Todd et al. (2008b) used a source analysis to confirm that the short-latency VsEPs are dominated by the pathways underlying the vestibular-ocular reflex, but also suggested activity in frontal cortex. More recently McNerney et al. (2011) used an alternative source analysis method to suggest that a wider range of vestibular cortical areas contribute to the short-latency potentials activated by sound. Such studies complement animal work using linear or rotational whole body acceleration to evoke short-latency vestibular responses (Sohmer et al., 1999; Jones et al., 2011).

While there is agreement on the existence of short-latency vestibular evoked effects, and some progress made in elucidating the sub-cortical and cortical generators in humans, a question which has not been addressed is the contribution, if any, made by vestibular receptors to the late auditory evoked potentials (LAEPs). These are characterised by a series of potentials, which are usually measured at the vertex, between about 50 and 250 ms, i.e. the P1, N1 and P2 (although the P1 is sometimes considered as a Pb wave following the mid-latency response (MLR) Na, Pa and Nb waves (Picton, 2011)). Source analysis indicates that the primary generators are bilateral tangential and radial sources in superior temporal cortex, with additional generators in the frontal cortex (Naatanen and Picton, 1987; Scherg et al., 1989). The aim of the present study was to address the above question by looking for evidence of changes in 500 Hz AC sound evoked LAEP when stimuli are presented at intensities above vestibular threshold and to carry out a source analysis.

2. Methods

2.1. Subjects

Fourteen healthy subjects were selected for this study (mean age = 28.3; SD = 6.9; 5 females and 9 males). All subjects were first screened for any neurological, vestibular and hearing impairment. Prior to any testing, all participants gave written informed consent according to the Declaration of Helsinki. The University of Manchester Research Ethics Committee approved the study.

2.2. Stimuli

The experimental stimuli employed for obtaining vestibular responses were AC 2-ms, 500-Hz, single cycle tone pips. AC stimuli were delivered by insert earphones (3A insert earphone, E-A-RTone Gold, Guymark UK Limited). The maximum input voltage, which was set to 1 V pp, resulted in a maximum output on the amplifier equivalent to a peak SPL of 135.9 dB re 20 μPa (as measured by the LLpk parameter with linear frequency weighting) and an RMS SPL of 115.4 dB re 20 μPa (measured by the LAI parameter, with A-frequency weighting and impulse time weighting). Stimulus calibration was carried out using a GRAS IEC711 Coupler (RA0045) and a pressure-field microphone (Model 4134) with a 2260 Investigator (Brüel and Kjaer, Naerum, Denmark). The stimuli were generated using customised software with a laboratory interface (power 1401, Cambridge Electronic Design, Cambridge, UK) and a commercial or custom amplifier.

2.3. Procedure

In normally hearing subjects use of AC stimuli will give rise to evoked potentials of cochlear origin, i.e. auditory evoked potentials (AEPs), and thus any vestibular evoked potentials (VsEPs) would be mixed in with AEPs. For this reason after obtaining the subjects' VEMP thresholds we recorded EEG responses both below and above the VEMP threshold in two separate sessions. The VEMP threshold is necessarily higher than the receptor threshold due to synaptic attenuation, but is convenient to use as it fairly easy to obtain and changes in the infra-ocular waveforms, i.e. presence and absence of OVEMPs, are clearly recognizable above and below this level. However although this threshold does not guarantee that the EEG response is free from vestibular influence we expected that they would be predominantly cochlear in origin.

2.4. Auditory thresholds

Audiograms were obtained for both ears using an Amplivox audiometer (Amplivox Ltd, UK) with Telephonics TDH 49 earphones (Telephonics Corp., Farmingdale, NY, USA). Each subject satisfactorily achieved pure tone air conduction thresholds of $\leq$20 dB HL at 125, 250, 500, 1000, 2000, 4000 and 8000 Hz bilaterally, according to British Society of Audiology (BSA) (2011) recommended procedures. The subjects had no history of otological or neurological pathology.

Psychophysical auditory thresholds of the stimulus used for evoked response recording were determined using PsyLab (v2.0, Hansen, 2006) using 3-alternative forced choice (3AFC), one-up two-down adaptive method to track the 79.4% point on the psychometric function (Levitt, 1971). The signal, i.e. 2-ms, 500-Hz, single-cycle tone-pip, was randomly presented to the subject in one of the three intervals and delivered unilaterally through insert earphones (3A insert earphone, E-A-RTone Gold, Guymark UK Limited). The initial signal level was set to 81 dB LLpk; this was reduced by 4 dB after two successive correct responses and increased by 4 dB after an incorrect response. After four reversals the measurement phase began and the step size was reduced to 1 dB. The threshold was taken as an average of the last four reversals.

2.5. Vestibular thresholds

Vestibular thresholds were obtained by means of VEMPs. Subjects were tested lying supine on a couch, with the backrest to

approximately tilted 30–45° from the horizontal, and lifted their heads against gravity to activate the sternocleidomastoid (SCM) muscles. Surface EMG was measured from the ipsilateral SCM using self-adhesive Ag/AgCl electrodes. Active surface electrodes were placed over the middle of the SCM muscle belly and were referred to electrodes placed on the medial clavicle. EMG was amplified, bandpass filtered (5 Hz–1 kHz) and sampled using a Power 1401 interface (CED Ltd., Cambridge, UK). The EMG was sampled at a rate of 5 kHz, starting 10 ms before to 80 ms following stimulus onset, and averaged. Stimuli were delivered by insert earphones (3A E-A-RTone Gold, Guymark UK Limited). Up to 200 stimuli were presented at a rate of about 6 Hz.

VEMP thresholds (V_T) were determined for each subject by reducing the stimulus intensity in 5 dB steps over successive trials and were defined as the smallest intensity at which a VEMP could be produced in at least two trials. The procedure was performed for left and right sides of stimulation independently.

2.6. VsEPs

VsEPs were recorded with subjects comfortably seated with their gaze directed straight ahead to a screen displaying silent movies at a viewing distance (about 70 cm). This recording position was adopted in order to avoid significant eye movement and alpha-wave artifact. AC pips were randomly presented between 600 and 1000 ms, up to a total of 400 stimuli per trial. Evoked potentials (EPs) were recorded in two test sessions; sub- and supra-threshold intensities were used in a first test session, i.e. −6, 0, +6, +12 and +18 dB re V_T, and only sub-threshold intensities were presented in a second part, i.e. −6, −12, −18 and −24 dB re V_T.

EEG was recorded using a 64-channel EEG system (Biosemi, Inc., USA). Additional electrodes were also placed below each eye (i.e. infra-ocular electrodes, IO1 and IO2), at deep frontal (F9 and F10) and at ear-lobe locations (A1 and A2). Electrode offset (i.e. running average of the voltage measured between CMS and each active electrode) was maintained below 20 μV. Recordings were made with a band-pass of between 0.16 Hz and 1 kHz. Artefact elimination, epoching and averaging of EPs were carried out using the BESA 5 software. Epochs were 350 ms in length, from 50 ms before to 300 ms following the stimulus onset. After collection, EPs were filtered at 1–200 Hz and referenced either to the ear-lobe electrodes or to an average reference using Scan software (v4.3, Neuroscan, USA). Amplitudes and latencies of mid and long-latency AEPs were measured at response peaks.

2.7. Source analyses

BESA software (version 5.1 MEGIS Software GmbH, Germany) was used for dipole modelling. The standard four-shell elliptical head approximation was employed with the following parameters. The radial thickness of the head, scalp, bone and CSF were 85, 6, 7 and 1 mm respectively with conductivities set to 0.33, 0.33, 0.0042 and 1.0, respectively. Prior to conducting the source analysis changes in the global field power with intensity were also evaluated in order to determine the appropriate fitting epoch.

3. Results

3.1. Auditory and vestibular thresholds

VEMP thresholds (V_T) were recorded in all healthy subjects, with a mean (SD) threshold of 108.7 (6.1) dB peak sound pressure level (pkSPL) and 109.3 (6.5) dB pkSPL for left and right air-conducted (AC) stimulation, respectively. Absolute auditory thresholds were 26.0 (5.3) dB pkSPL and 26.2 (4.1) dB pkSPL for left and right AC stimulation, respectively. Combined together these are equivalent to 82.7 and 83.1 dB sensation level (SL), similar values to that found by Todd et al. (2008b). As noted in the methods section the vestibular receptor threshold is likely to be below this, possibly by as much as 10 dB or more, i.e. at around 70 dB SL (Todd et al., 2010).

3.2. Properties of the averaged electroencephalography (EEG)

Grand means for the major conditions are illustrated in Figs. 1 and 2. Sub-threshold conditions (−12, −18 and −24 dB re V_T)

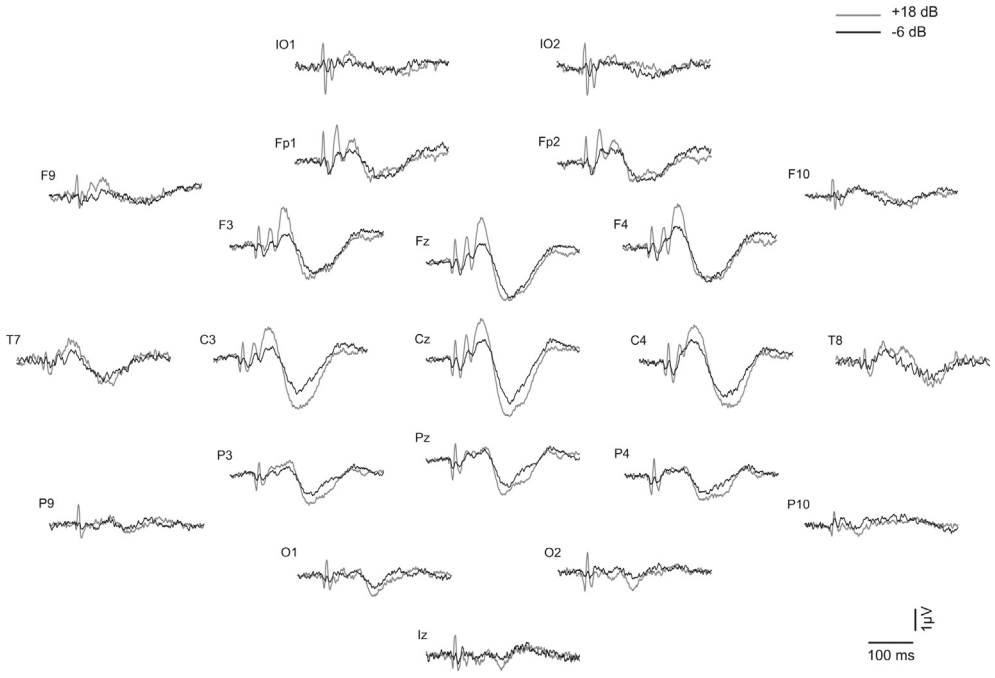

Fig. 1. Grand means of evoked potentials produced by 500-Hz 2-ms pips in standard 10–20 locations, plus infra-ocular (IO), F9, F10, P9 and P10. For each of the electrode locations the two traces show the +18 dB re V_T (grey trace) vs. the −6 dB re V_T (black trace) conditions.

produced a typical auditory brainstem response (ABR) and middle/long-latency auditory evoked response (MLR/LAER) pattern consisting of the slow wave V followed by the Na, Pa, Nb, Pb/P50/P1, N1, P2 waves. These were well illustrated in channel FCz (Fig. 2, AEPs indicated with grey labels). In contrast, supra-threshold conditions (+6, +12, +18 dB re V_T) produced responses with an altered morphology.

The altered morphology includes short-latency waves (Todd et al., 2008b). These waves are clearest in the infra-ocular (IO), prefrontal (Fpz) and inion (Iz) leads (Fig. 2, VsEPs indicated with

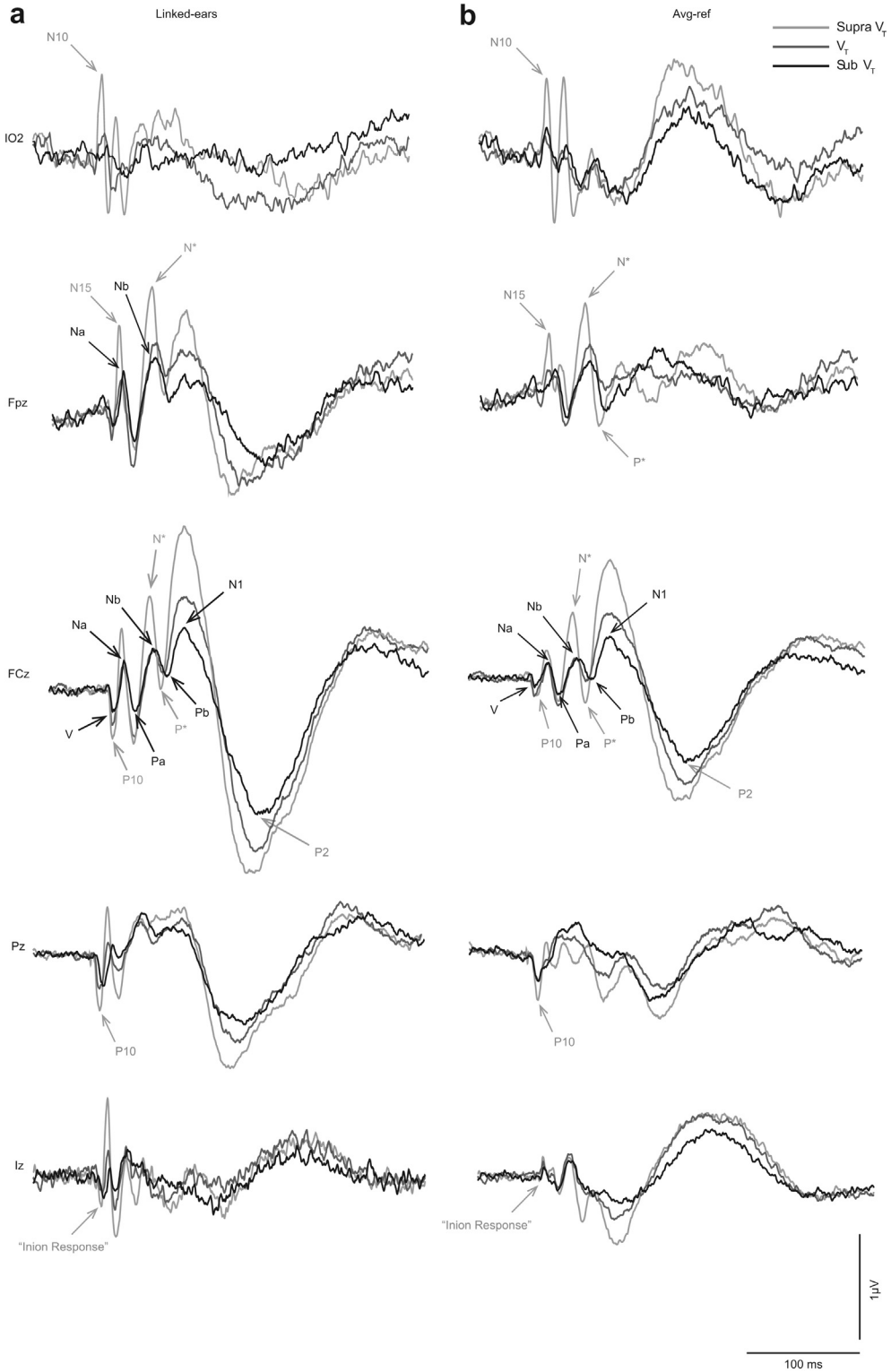

Fig. 2. Grand means of evoked potentials produced by left ear presented 500-Hz 2-ms pips from the electrode positions IO2, Fpz, FCz, Pz and Iz for both (a) linked-ears reference and (b) average reference. For each panel the three traces indicate sub-threshold (black), threshold (dark grey) and supra-threshold (light grey) intensities. AEPs are indicated in light grey, VsEPs in black.

black labels). The IO responses consist of a series of alternating waves, the earliest of which occurs at 10 ms and is referred to as an N10 (Todd et al., 2008b). The polarity and latency of these waves correspond with OVEMPs measured using a differential montage (Todd et al., 2007). In the prefrontal lead (Fpz), an N15 (Todd et al., 2008b) with similar latency to the latency of Na component of MLR is apparent. In the parietal lead, a positivity at about 10 ms is present. Such positivity has conventionally been referred to as P10 (Todd et al., 2008b), although this tends to merge with the wave V of the ABR after low-pass filtering at 200 Hz. In the inion lead (Iz), a series of waves analogous to the IO waves can be observed, the earliest occurring at about 10 ms.

In addition to the above, some additional later waves not previously described were also observed. In particular a prominent prefrontal negativity (labelled "N*" in Fig. 2) with similar latency to the Nb component of MLR was apparent, followed by a corresponding positivity (labelled "P*") with a similar latency to the Pb/P1 deflection of the MLR/LAER, but with a more definitely positive character than for the sub-threshold condition. This N*–P* deflection could be observed clearly in the midline frontal electrodes, Fpz and FCz. A further change in morphology was observed in the later waves with enhancement of the N1 potential compared to the P2.

As the transition from Nb/Pb to N*/P* is quite a subtle one in the grand mean we also illustrate in Fig. 3 the transition in the individual responses at leads IO2 and FCz when passing through the VEMP threshold. At −6 dB re V_T there is little or no sign of the OVEMP waveform in the individual traces, although there is a hint of a small OVEMP in the grand mean. Similarly at FCz there is no consistent Nb/Pb deflection, but a hint in the grand mean. At +18 dB re V_T in contrast both OVEMP and N*/P* waveform are consistently present in the individual traces, with the peak–peak OVEMP and N*/P* amplitudes being approximately the same.

3.3. Changes in the averaged EEG with stimulus intensity

In order to investigate statistically the effects of stimulus intensity on the amplitude of the responses, we measured peak–peak values of the potentials at the latency of the Pa–Nb and Nb–Pb components of MLRs (including the N*P* components: Fig. 4a,b), and the peak values of the N1 and P2 components of LAERs (Fig. 4c,d), for stimuli presented at −24, −18, −12, −6, 0, +6, +12, and +18 dB re V_T. As there was no significant difference in the −6 dB condition recorded at two separate sessions, the average value of the two was used.

Fig. 4 shows amplitude vs. intensity functions for MLRs and LAERs. The slopes show clear departures from linearity as they pass through the vestibular threshold. In order to quantify this we carried out a slope analysis by means of linear regression of both individual amplitudes and grand mean amplitudes for the sub- (−24, −18, −12 and −6 dB) vs. supra-threshold (0, +6, +12 and +18 dB) conditions. A t-test ($n = 14$, $\alpha = .05$, two-sided) to compare the sub- vs. supra-threshold regression parameters for each wave yielded essentially the same result, which was that the MLR peak–peak amplitudes showed a significant increase in slope (at the 5% level) when passing through the vestibular threshold. For the Pa–Nb the slope changed from 12 to 42 nV per dB ($p = .042$) and for the Nb–Pb (N*–P*) from −10–39 nV per dB ($p = .003$). For the N1 and P2 potentials there was no significant change in slope.

In addition to the slope analysis ANOVAs were carried out separately on the amplitudes for the MLR and LAER amplitudes with within-subjects factors of "wave" (Pa–Nb and Nb–Pb for the MLR and N1/N74 and P2 for the LAER) and "intensity" (+18, +12, +6, 0, −6, −12, −18 dB re V_T). For the MLR epoch the ANOVA yielded a main effect of intensity ($F_{(7, 91)} = 15.6$, $p < .001$) and a significant linear contrast ($F_{(1, 13)} = 46.3$, $p < .001$), but also a significant quadratic contrast ($F_{(1, 13)} = 9.0$, $p < .05$), consistent with the slope change detected above. For the LAER amplitudes the ANOVA also yielded a main effect of intensity ($F_{(7, 91)} = 12.5$, $p < .001$) and a linear contrast ($F_{(1, 13)} = 21.5$, $p < .001$), but in this case a significant 5th order contrast ($F_{(1, 13)} = 6.1$, $p < .05$) indicating a more complex slope pattern.

Changes in the latencies of Pa, Nb/N*, Pb/P*, N1 and P2 with intensity are shown in Fig. 5. All waves show a general trend of decreased latency with increase in intensity, with a shallowing slope. ANOVAs carried out separately for each of the waves in the range of −12 to +18 dB confirmed that the Nb/N* and Pb/P* each showed significant main effects of intensity, ($F_{(5, 65)} = 6.7$, $p < .01$) and ($F_{(5, 65)} = 5.2$, $p < .05$) respectively. There was a shift in latencies with increase in stimulus intensity, from 50.3 to 42.1 ms for the Nb/N* and from 60.6 to 52.8 ms for the Pb/P*, both by about 8 ms. In contrast the MLR Pa and the LAER N1 and P2 latencies did not show any significant effects, indicating that the intensity function had reached its asymptote for these waves.

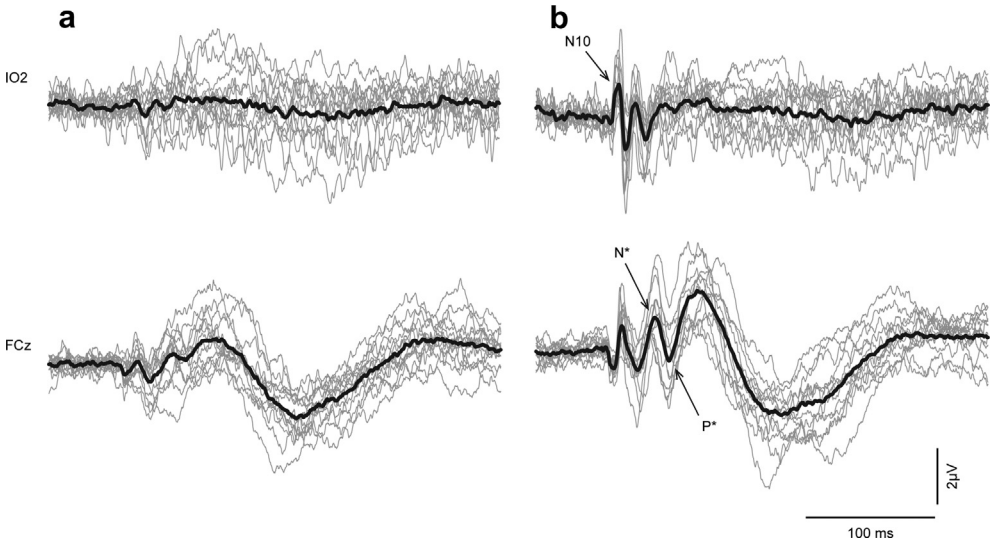

Fig. 3. Individual traces (light grey) of each of the 14 subjects compared with the grand mean (black) at IO2 and FCz electrodes for (a) −6 dB re V_T and (b) +18 dB re V_T.

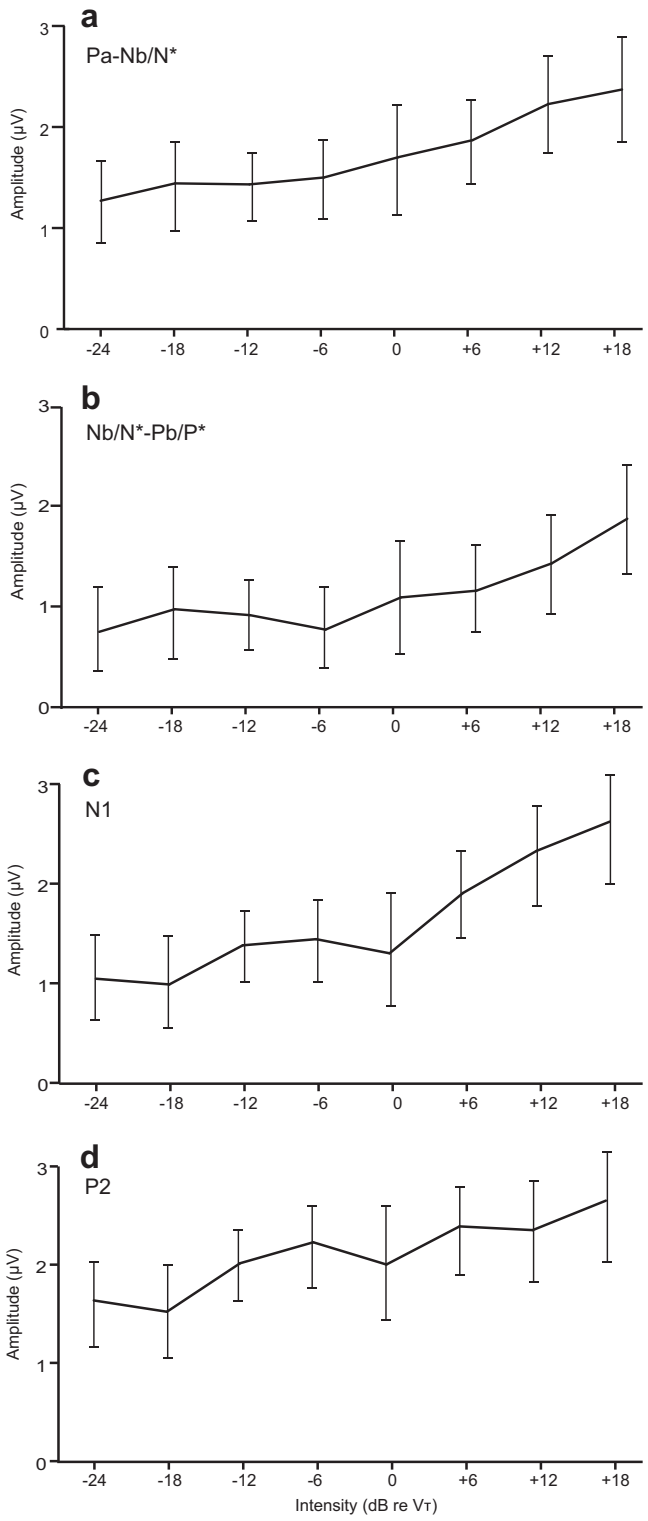

Fig. 4. Amplitude as a function of intensity, (a) peak–peak Pa–Nb/N*, (b) Nb/N*–Pb/P*, (c) N1 and (d) P2. The intensity increases in 6 dB steps from −24 to +18 dB re V_T.

3.4. AEPs in a patient with unilateral vestibular loss

Fig. 6 illustrates the effect of unilateral vestibular loss on VsEPs. This patient had a history of vestibular dysfunction with absent VEMPs for right side AC stimulation. His low-frequency audiogram was normal for this ear. Comparison of the waveforms of AC evoked responses in selected EEG leads with the average response in a sample of normal subjects on right ear stimulation shows clear differences. AEPs are mostly intact in the patient whereby waves V, Na, Pa, N1 and P2 are well-formed. In contrast there is absence of the OVEMP waveform in IO2, the N15 and N* components in Fpz, the N*–P* deflection at FCz, the P10 component at Pz and the inion response at Iz.

3.5. Changes in the global field power and scalp distribution

Fig. 7 illustrates the changes in the GFP with intensity, which mirror the changes in morphology noted above. At intensities below V_T four lobes of the GFP can be discerned which correspond to AEPs Na, Pa, N1 and P2. At the highest intensity, in contrast, six distinct lobes can be discerned. The earliest three of these have been previously described and correspond primarily to activities associated with short-latency VsEPs, which are dominated by VEMP sources (Todd et al., 2008b). The last two late lobes correspond to the AEP N1 and P2 wave. The lobe preceding the N1 activity is not present in the sub-threshold conditions and corresponds to the growth of the N* deflection described above. At sub-threshold intensities there is no particular focus in the scalp map but with an increase in intensity the N* develops two midline foci, one at Fpz and the other at FCz.

3.6. Source analysis

Given the novelty of the N*–P* deflection we focused the source analysis to the lobe of the GFP associated with this activity, i.e. between approximately 32 and 52 ms, the latencies of the minima either side of the 4th lobe. The modelling strategy employed was to start with the simplest models and gradually build up complexity using a genetic algorithm in which the number of sources could be specified. Source analysis was carried out on unfiltered grand averages. The results of this analysis are given in Table 1.

For the simplest models, i.e. 1, 2 or 3 dipoles, a unique solution could be obtained which indicated that 90% of the variance could be explained by contributions from an ocular source and from a cortical midline source in a middle cingulate location. The third source, which was located to a deep area, explained just an additional 3% of variance. All three sources were contralateral to the midline. For more than 3 sources no unique solution could be obtained, but a number of additional sources were indicated, including a contralateral cortex source and a cerebellar source, as well as a deep source indicated in the unique solutions.

Since an ocular source was implicated we also investigated a set of models in which a single dipole was replaced by a symmetrical pair, with an additional 2, 3 or 4 sources. All three of these models located the ocular pair within the orbit, and again located a second source in the midline, with additional sources in contralateral, cerebellar and deep locations. For an ocular pair and three dipoles the residual variance was reduced to 4.2%. An example of two of these solutions is illustrated in Fig. 8. As the ocular sources are likely to be complex, including possibly a combination of VEMP and EOG signals, we also investigated a class of model in which the ocular pair of dipoles was replaced by a pair of regional sources. Stable and interpretable solutions were obtainable with an additional one and two dipoles. As above the first dipole was always located to the midline in a cingulate region with the second to a contralateral region.

Examination of the morphology of the midline current source (sources 3 and 5 in Fig. 8b) suggests that its activity is not confined to the fitting interval employed but continues to contribute significantly to the later components. In order to investigate this further we also carried out a source analysis of the 5th lobe of the GFP associated with the N1, i.e. for the interval 52–102 ms, independently of the 4th lobe. A standard approach to modelling the N1

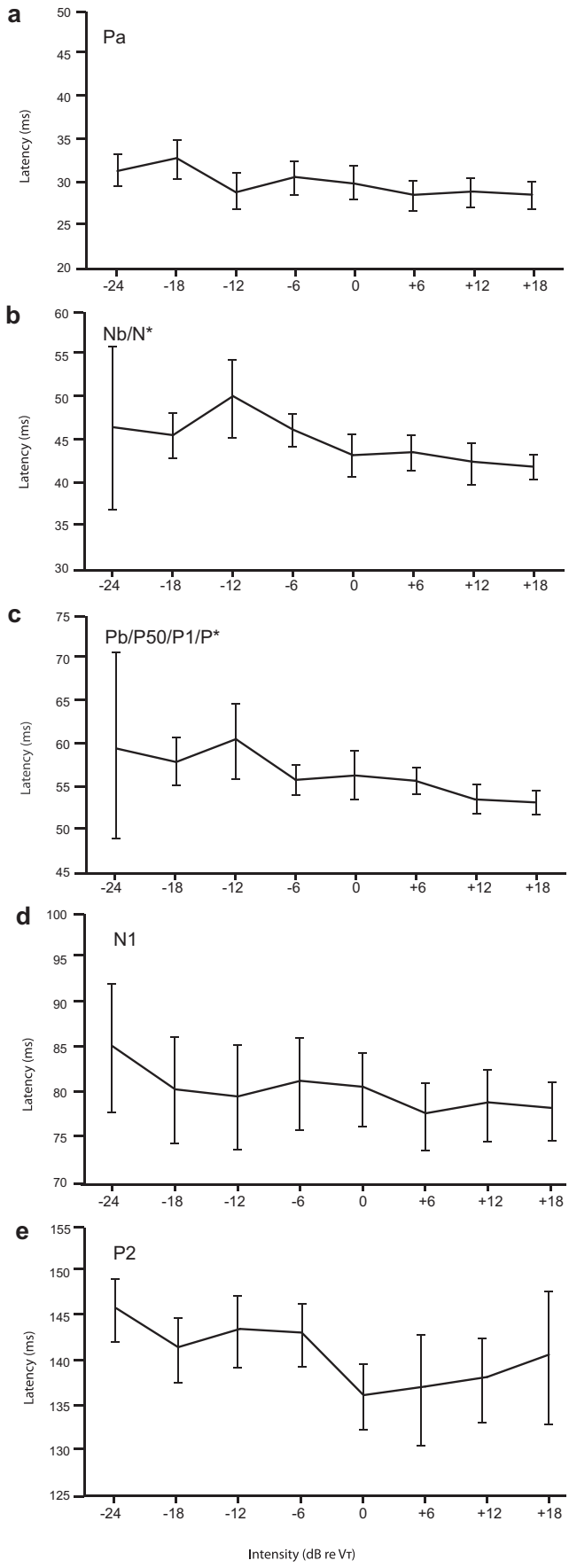

Fig. 5. Latency as a function of intensity, (a) Pa, (b) Nb/N*, (c) Pb/P50/P1/P*, (d) N1 and (e) P2.

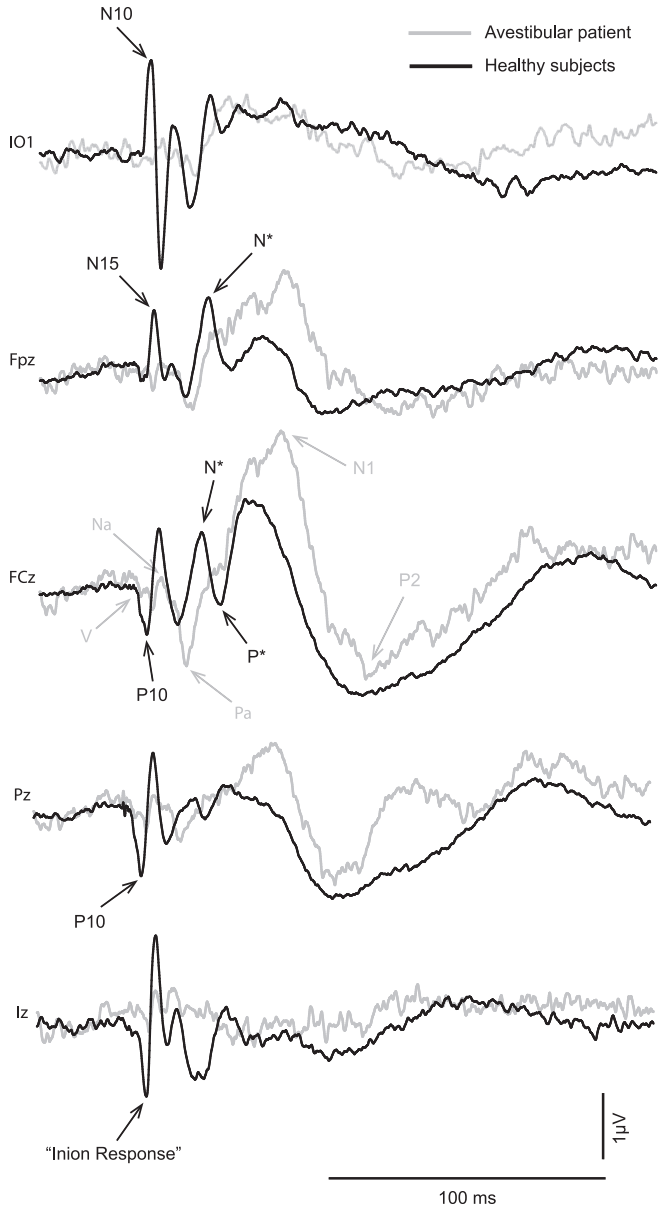

Fig. 6. Grand means of evoked potentials produced by right-ear presented 500-Hz 2-ms pips in 10 healthy subjects (black) vs. a unilaterally avestibular patient (grey). Traces are shown from the electrode positions IO2, Fpz, FCz, Pz and Iz.

is to fit a pair of regional sources. We applied this approach, as well the simple dipole source approach employed above.

About 94% of the variance could be explained with just two dipoles, one located in the contralateral temporal lobe and the other in a midline position. With three dipoles the ipsilateral temporal lobe was also implicated, along with the midline and contralateral sources. If a pair of regional sources was applied, the resultant locations were medial of temporal lobe, indicative of the presence of an additional midline source. Thus, for a symmetrical pair of regional sources and a single dipole (illustrated in Fig. 8c), the regional sources were located within the bilateral transverse temporal gyrus (±53, −19, 8) with the single source located to the mid-cingulate area, accounting for about 97% of variance. Consistent with the single dipole approach, the largest current is from the mid-line source, followed by the contralateral source, with a relatively small contribution from the ipsilateral source.

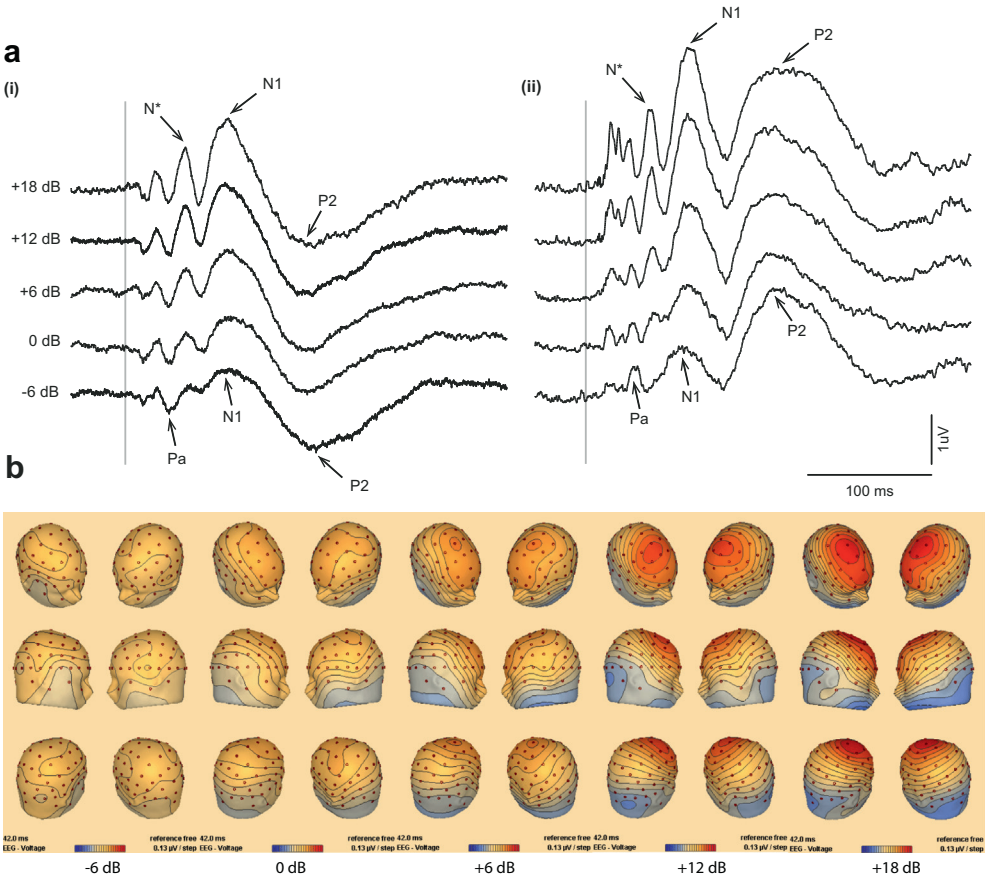

Fig. 7. Changes in the scalp potentials as a function of intensity from −6 dB to +18 dB re VT. (a) (i) Voltage measured at FCz vs. (ii) associated global field power (GFP) and (b) scalp map at 42 ms.

4. Discussion

In the present study, we have provided evidence that for 500-Hz AC-stimuli there are systematic changes that take place in LAEPs at intensities above the VEMP threshold and have tentatively identified a new mid-latency potential which appears to have a significant vestibular contribution. The changes that take place are of two kinds: changes in the slope of the amplitude functions with intensity of the AC stimulus and changes in the morphology and distribution of the potentials above and below V_T. We discuss each of these below.

There are a number of prior studies that indicate AEPs tend to plateau and saturate with increasing intensity. For the Pb component saturation occurs at quite low intensity, from about 50 to 70 dB normal Hearing Level (nHL) (Thornton et al., 1977; Ozdamar and Kraus, 1983), while for the N1/P2 components saturation occurs at higher levels, i.e. at about 80–90 dB nHL (Picton et al., 1974; Dierks et al., 1999; Picton, 2011). Our data also show evidence of early saturation of the Pa–Nb and Nb–Pb components in the form of a plateau up to the vestibular threshold, consistent with the earlier literature, but then this is followed by an increase in slope at around the vestibular threshold where the N*–P* component is recruited. Although the N1/P2 waves in our case do not show a significant change in slope they do exhibit a plateau or inflexion near the vestibular threshold (about 80 dB SL) followed by a continued increase in amplitude.

Prior studies of changes in the latency of AEPs as a function of intensity are consistent in revealing a general tendency of the latency to reduce with intensity but with a decreasing rate of change (slope) as intensity increases, possibly to a point of saturation, i.e. where there is no further significant change. For the Na/Pa waves a saturation may occur early at about 40–50 dB nHL (Maurizi et al., 1984), but for the N1/P2 component, although the largest change in slope takes place up to 40 dB nHL, the latency continues to decrease up to 90 dB nHL, albeit at a slower rate (Picton, 2011). Prior studies of the Pb component, however, indicate a more complex non-monotonic latency-intensity function (Ozdamar and Kraus, 1983). In our results we detected a significant latency shift in the Nb/N* and the Pb/P* components in passing through the vestibular threshold, but not for the Na or the N1 and P2 components. This result supports an interpretation that the Na, N1 and P2 components of the AEP had reached near saturation but an additional process was occurring in the generators responsible for the N*–P* deflection.

Considering the changes in waveform morphology, the most dramatic change around V_T occurs in the infra-ocular and inion leads with the appearance of OVEMP and inion response waveforms. However, in addition to these changes, there was also the development of the N*–P* deflection. The avestibular patient had absent OVEMP, N15, P10, and inion responses and also lacked the N*–P* deflection. These two waves also showed a significant increase in the peak–peak slope in the amplitude function of intensity and a significant change in their latency in passing through the vestibular threshold. Taken together with the latency changes, our evidence supports the view that the N*–P* deflection is vestibular in origin. For this reason we refer to these hereafter as vestibular N42/P52 waves, in order to distinguish them from their AEP counterparts the Nb/Pb waves. The Pb or P50 when considered with the LAERs is referred to as a P1, preceding the N1 and P2. Thus our data supports the case that vestibular receptors do indeed contribute to the LAERs, which are believed to be cortical in origin,

Table 1
Summary of source analysis models for the 4th lobe of the GFP (32–52 ms).

Model	Number of sources	R^2	TTCs	Region	Possible origin
Simple Dipole	1 DP	18%	10, 15, −7	–	–
	2 DPs	9.8%	16, 56, −39,	Ocular	R OVEMP/Eye movement
			3,−9, 34	Midline	R Cingulate/BA24
	3 DPs	6.9%	12, 65, −43	Ocular	R OVEMP/Eye movement
			8, −20, 33	Midline	R Cingulate/BA24
			47, −22, −57	Deep	R Neck/Brainstem/Cerebellum
	4 DPs Version 1	5.9%	13, 67, −42	Ocular	R OVEMP/Eye movement
			18, −5, 42	Midline	R Cingulate/BA24,31
			9, −45, 21	Deep	Brainstem
			44, −24, −57	Posterior	Inion/Cerebellum
	4 DPs Version 2	5.9%	12, 65, −43	Ocular	R OVEMP/Eye movement
			18, −5, 42	Midline	R Cingulate/BA24,31
			9, −45, 21	Midline	R Posterior Cingulate/BA30,23,29,31
			44, −24, −57	Deep	R Neck/Brainstem/Cerebellum
	4 DPs Version 3	5.7%	34, 65, −21	Ocular	R OVEMP/Eye movement
			26, 61, −42	Ocular	L OVEMP/Eye movement
			8, −20, 33	Midline	R Cingulate/BA24
			37, −51, −13	Contralateral	R Temporal/Occipital/Cerebellum/BA37
Symmetrical Pair & Simple Dipole	Pair & 2 DPs	6.0%	±26, 58, −28	Ocular	L & R OVEMP/Eye movement
			7, −19, 33	Midline	R Cingulate/BA23,24,31
			40, −47, −18	Contra	R Cerebellum/Temporal/BA37
	Pair & 3 DPs	4.8%	±21, 62, −45	Ocular	L & R OVEMP/Eye movement
			19, −6, 37	Midline	R Cingulate/BA24
			24,−53, 16	Contralateral	R Temporal/Posterior Cingulate/BA31
			19, −72, −41	Posterior	R Cerebellum
	Pair & 4 DPs	4.2%	±25, 60, −46	Ocular	L & R OVEMP/Eye movement
			19, −9, 35	Midline	R Cingulate/BA24
			25, −59, 21	Contralateral	R TPO/Posterior Cingulate/BA31
			−6, −73, −27	Posterior	L Cerebellar Vermis
			6, −4, −55	Deep	Brainstem
Regional Source Pair & Simple Dipole	2 RS & 1 DP	6.8%	±28, 58, −33	Ocular	L & R OVEMP/Eye movement
			8, −20, 36	Midline	R Cingulate/BA24,23,31
	2 RS & 2 DPs	4.9%	±31, 63, −22	Ocular	L & R OVEMP/Eye movement
			9, −20, 32	Midline	R Cingulate/BA24,23,31
			40, −47, −18	Contralateral	R Occipital/Cerebellum/Temporal/Parahippocampal/BA37,19

Abbreviations: Brodmann Area (BA), Dipole (DP) Left (L) Ocular Vestibular Evoked Myogenic Potential (OVEMP), Regional Source (RS), Right (R), Temporal/Parietal/Occipital (TPO), Talairach–Tournoux Coordinates (TTC).

and thereby provides a new method of investigating vestibular-cortical projections in intact human subjects.

Although source analysis cannot establish definitively a causal locus or generator site it is a useful method for providing hypotheses for such sites. Our analysis implicated mid-cingulate activity, along with a source emanating from the eyes, as accounting for 90% of the variance associated with the N42/P52, and, along with contralateral auditory cortex, accounting for 94% of the LAEP N1. The recruitment of cingulate cortex above vestibular threshold plausibly accounts for the changes in slope we observed in the amplitude-intensity functions of both N42 and N1. Activity within the cingulate gyrus is consistent with the literature on vestibular cortical projections in which a "vestibular cingulate region" has been identified in primate studies (Guldin and Grusser, 1998). In humans the vestibular cingulate area extends from anterior cingulate to middle and more posterior cingulate areas (Lopez and Blanke, 2011). In our case the source was located in a mid-cingulate area (TTC y-coordinate ranging from −5 to −20) corresponding approximately with the posterior aspect of BA24 (anterior cingulate) and anterior portions of BA 23 and 31 (posterior cingulate). A number of imaging studies using caloric and galvanic vestibular stimulation have observed activity in this area; (Lobel et al., 1998; Suzuki et al., 2001; Fasold et al., 2002). Recent attempts that have been made using fMRI with acoustic stimulation to investigate saccular cortical projections have also observed cingulate activation. Miyamoto et al. (2007) reported activation in both the anterior (BA32) and posterior cingulate (BA31) although this was not replicated by Schlindwein et al. (2008).

The anterior cingulate region is considered to have two distinct functional and anatomic divisions, i.e. dorsal/rostral vs. ventral/caudal (Lopez and Blanke, 2011). The dorsal cingulate is generally associated with motor function, including ocular-motor control, and is connected with frontal eye fields, PIVC and other vestibular areas (Guldin and Grusser, 1998). The ventral portion is considered to be more limbic in function, and is connected to anterior insula and other subcortical structures. Of particular relevance to the present work was a study by Smith et al. (2012) who showed that there are strong cross-modal visual-vestibular interactions in an area they termed the cingulate sulcus visual area (CSv) which is "closely involved in encoding egomotion" and "strongly responsive to coherent optic flow". The CSv is in close proximity to the location of our cingulate source. This is consistent with a study by Antal et al. (2008), which showed activity in both cingulate cortex and planum temporale to coherent visual motion.

The existence of a vestibular contribution to AEPs, if confirmed, has at least two important consequences. The first is that any auditory studies, which make use of high signal intensity need to take into account the possibility that results are contaminated with

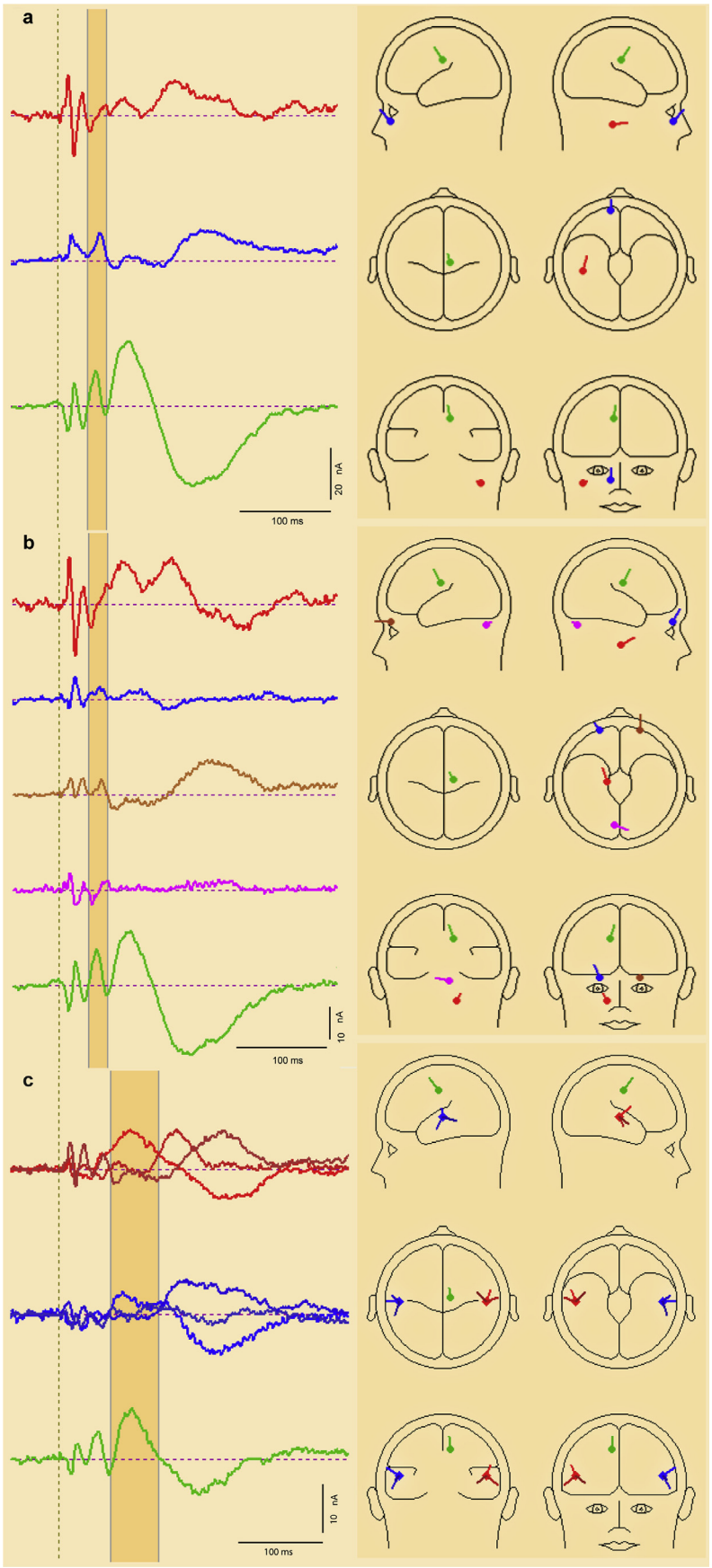

Fig. 8. BESA solutions for the 4th and 5th lobes of the GFP corresponding with N*–P* and N1 deflection. Source waveforms (i) and source locations and orientations (ii) are shown for (a) a 4th lobe 3 dipole model, (b) a 4th lobe model based on an ocular pair and 3 dipoles and (c) a 5th lobe 3 source model based on a pair of regional sources and a single dipole.

non-cochlear contributions. For example, a large number of studies make use of the loudness dependence of AEPs (LDAEP) to make inferences about the activity of certain catecholamine transmitters, including serotonin and dopamine (Dierks et al., 1999). Such methods have been applied to a number of psychiatric disorders, including depression, schizophrenia and obsessive-compulsive disorder. It is possible that the LDAEP results are influenced by activation of the vestibular system, especially as it appears that the highest intensity stimuli used in these studies, which may exceed 100 dB SPL, are the most critical (Gallinat et al., 2000). This is of particular importance because the central projections of the vestibular system include insular, cingulate and autonomic pathways, which employ transmitters of interest (Balaban and Yates, 2004; Lopez and Blanke, 2011).

A second potential consequence is that it is quite possible that acoustically activated non-cochlear (vestibular) projections may play a role in normal hearing, for example, in the vocal behaviour of primate and amniote vertebrate species (Todd and Cody, 2000; Todd and Merker, 2004; Todd, 2007), as well as the vocal behaviour of anamniotes for which the otolith organs are established as auditory. In the case of humans many music environments, such as at concerts, are of high-intensity and well above the threshold levels we have considered (Todd and Cody, 2000). Similarly, the singing voice is high-intensity and very likely produces self-activation of the vestibular apparatus (Todd, 1993) as was suggested as long ago as the 1930s by Tait (1932). Given a probable role of cingulate cortex, such activation could contribute to the affective responses to sound or in listening to music (Todd, 2001).

As noted above, the VEMP threshold overestimates the receptor threshold. McCue and Guinan (1994) found a rate threshold in cat vestibular afferents of 90 dB SPL for 50 ms tones, with a phase-locking threshold 10 dB lower. Combined with the appropriate psychophysical correction for short tone bursts, e.g. Meddis and Lecluyse (2011), this places the receptor rate threshold at near 70 dB SL. It is likely, therefore, that vestibular receptors contribute at intensities well below those experienced in the loud environments described in the previous paragraphs. The presence at everyday intensities of a vestibular component in cortical potentials from the temporal lobe, hitherto considered purely cochlear in origin, raises the possibility that acoustic activation of the otolith organs could contribute directly to auditory discrimination, as well as to affective processes. There is now a growing literature which provides evidence of a central vestibular–auditory interaction which allows vestibular inputs to improve temporal and spatial aspects of hearing (Emami and Daneshi, 2012; Brimijoin and Akeroyd, 2012; Probst and Wist, 1990), to contribute to speech perception and in metrical aspects of musical perception (Emami et al., 2012; Phillips-Silver and Trainor, 2008), and which indicates a general association between hearing loss and vestibular dysfunction (Akin et al., 2012; Zuniga et al., 2012; Kumar et al., 2010; Wang and Young, 2007). Given the well-established cross-over from vestibular to auditory pathways at the level of the brain-stem, (e.g. Barker et al., 2012), and thalamus, (Roucoux-Hanus and Boisacq-Schepens, 1977; Blum et al., 1979), vestibular effects at the level of temporal cortex should be expected, especially as activation of superior temporal lobe is consistently indicated in vestibular imaging studies (Lopez et al., 2012).

5. Concluding remarks

We have in this paper presented evidence to support a vestibular contribution to AEPs, and have tentatively identified a possible new component, the N42/P52, which appears to be vestibular in origin. Some of this evidence is quite subtle, but this probably explains why it has hitherto not been remarked upon. However, given the potential implications of the vestibular–auditory interaction for hearing research it is important that further work is conducted to substantiate these. Among the most important of these future studies should be work with a larger sample of avestibular patients to investigate differences in AEPs. Given also the limitations of the VEMP threshold in identifying a receptor threshold new methods for establishing a N42/P52 threshold directly from AEPs should be developed. Finally higher resolution imaging methods will be required to substantiate the brain areas suggested by the BESA.

Acknowledgements

The research reported in this article was supported by a grant from the Wellcome Trust (WT091961MA). We are grateful to Sendhil Govender for assistance in recording EEG from the vestibular patient and to Dr M Welgampola and Professor M Halmagyi for their cooperation in the recruitment of the patient. We would like to thank Prof Chris Plack and Dr Selvino de Kort for their comments on an earlier version of this manuscript. We would also like to thank Aisha Mclean for assistance in the preparation of the manuscript.

References

Akin, F.W., Murnane, O.D., Tampas, J.W., Clinard, C., Byrd, S., Kelly, J.K., 2012. The effect of noise exposure on the cervical vestibular evoked myogenic potential. Ear Hear. 33, 458–465.
Antal, A., Baudewig, J., Paulus, W., Dechent, P., 2008. The posterior cingulate cortex and planum temporale/parietal operculum are activated by coherent visual motion. Vis. Neurosci. 25, 17–26.
Balaban, C.D., Yates, B.J., 2004. Vestibuloautonomic interactions: a teleologic perspective. In: Highstein, S.M., Fay, R.R., Popper, A.N. (Eds.), The Vestibular System. Springer-Verlag, New York, pp. 286–342.
Barker, M., Solinski, H.J., Hashimoto, H., Tagoe, T., Pilati, N., Hamann, M., 2012. Acoustic overexposure increases the expression of VGLUT-2 mediated projections from the lateral vestibular nucleus to the dorsal cochlear nucleus. PLoS One 7.
Bickford, R.G., Jacobson, J.L., Cody, D.T.R., 1964. Nature of average evoked potentials to sound and other stimuli in man. Ann. N. Y. Acad. Sci. 194, 112–204.
Blum, P.S., Day, M.J., Carpenter, M.B., Gilman, S., 1979. Thalamic components of the ascending vestibular system. Exp. Neurol. 64, 587–603.
Brimijoin, W.O., Akeroyd, M.A., 2012. The role of head movements and signal spectrum in an auditory front/back illusion. i-Perception 3, 179–182.
Colebatch, J.G., Halmagyi, G.M., Skuse, N.F., 1994. Myogenic potentials generated by a click-evoked vestibulocollic reflex. J. Neurol. Neurosurg. Psychiatry 57, 190–197.
Curthoys, I.S., Kim, J., McPhedran, S.K., Camp, A.J., 2006. Bone conducted vibration selectively activates irregular primary otolithic vestibular neurons in the guinea pig. Exp. Brain Res. 175, 256–267.
de Waele, C., Baudonniere, P.M., Lepecq, J.C., Huy, P.T.B., Vidal, P.P., 2001. Vestibular projections in the human cortex. Exp. Brain Res. 141, 541–551.
Dierks, T., Barta, S., Demisch, L., Schmeck, K., Englert, E., Kewitz, A., Maurer, K., Poustka, F., 1999. Intensity dependence of auditory evoked potentials (AEPs) as biological marker for cerebral serotonin levels: effects of tryptophan depletion in healthy subjects. Psychopharmacol 146, 101–107.
Emami, S.F., Daneshi, A., 2012. Vestibular hearing and neural synchronization. ISRN Otolaryngol.. http://dx.doi.org/10.5402/2012/246065.
Emami, S.F., Pourbakht, A., Sheykholeslami, K., Kamali, M., Behnoud, F., Daneshi, A., 2012. Vestibular hearing and speech processing. ISRN Otolaryngol.. http://dx.doi.org/10.5402/2012/850629.
Fasold, O., von Brevern, M., Kuhberg, M., Ploner, C.J., Villringer, A., Lempert, T., Wenzel, R., 2002. Human vestibular cortex as identified with caloric stimulation in functional magnetic resonance imaging. Neuroimage 17, 1384–1393.
Gallinat, J., Bottlender, R., Juckel, G., Munke-Puchner, A., Stotz, G., Kuss, H.J., Mavrogiorgou, P., Hegerl, U., 2000. The loudness dependency of the auditory evoked N1/P2-component as a predictor of the acute SSRI response in depression. Psychopharmacol. 148, 404–411.
Guldin, W.O., Grusser, O.J., 1998. Is there a vestibular cortex? Trends Neurosci. 21, 254–259.
Jones, T.A., Jones, S.M., Vijayakumar, S., Brugeaud, A., Bothwell, M., Chabbert, C., 2011. The adequate stimulus for mammalian linear vestibular evoked potentials (VsEPs). Hear. Res. 280, 133–140.
Kumar, K., Vivarthini, C.J., Bhat, J.S., 2010. Vestibular evoked myogenic potential in noise-induced hearing loss. Noise Health 12, 191–194.
Lackner, J.R., Graybiel, A., 1974. Elicitation of vestibular side-effects by regional vibration of head. Aerosp. Med. 45, 1267–1272.
Levitt, H., 1971. Transformed up-down methods in psychoacoustics. J. Acoust. Soc. Am. 49, 467–477.

Lewis, E., Narins, P. (Eds.), 1999. Comparative Hearing: Fish and Amphibians. Springer-Verlag, New York.
Lobel, E., Kleine, J.F., Le Bihan, D., Leroy-Willig, A., Berthoz, A., 1998. Functional MRI of galvanic vestibular stimulation. J. Neurophysiol. 80, 2699–2709.
Lopez, C., Blanke, O., 2011. The thalamocortical vestibular system in animals and humans. Brain Res. Rev. 67, 119–146.
Lopez, C., Blanke, O., Mast, F.W., 2012. The human vestibular cortex revealed by coordinate-based activation likelihood estimation meta-analysis. Neurosci. 212, 156–179.
Manley, G., Popper, A., Fay, R. (Eds.), 2004. Evolution of the Vertebrate Auditory System. Springer-Verlag, New York.
Maurizi, M., Ottaviani, F., Paludetti, G., Rosignoli, M., Almadori, G., Tassoni, A., 1984. Middle-latency auditory components in response to clicks and low- and middle-frequency tone pips (0.5–1 kHz). Audiology 23, 569–580.
McCue, M.P., Guinan, J.J., 1994. Acoustically responsive fibres in the vestibular nerve of the cat. J. Neurosci. 14, 6058–6070.
McKnight, C.L., Doman, D.A., Brown, J.A., Bance, M., Adamson, R.B.A., 2013. Direct measurement of the wavelength of sound waves in the human skull. J. Acoust. Soc. Am. 133, 136–145.
McNerney, K.M., Lockwood, A.H., Coad, M.L., Wack, D.S., Burkard, R.F., 2011. Use of 64-channel electroencephalography to study neural otolith-evoked responses. J. Am. Acad. Audiol. 22, 143–155.
Meddis, R., Lecluyse, W., 2011. The psychophysics of absolute threshold and signal duration: A probabilistic approach. J. Acoust. Soc. Am. 129, 3153–3165.
Miyamoto, T., Fukushima, K., Takada, T., de Waele, C., Vidal, P.-P., 2007. Saccular stimulation of the human cortex: a functional magnetic resonance imaging study. Neurosci. Lett. 423, 68–72.
Naatanen, R., Picton, T., 1987. The N1 wave of the human electric and magnetic response to sound – a review and analysis of the component structure. Psychophysiol. 24, 375–425.
Ozdamar, O., Kraus, N., 1983. Auditory middle-latency responses in humans. Audiology 22, 34–49.
Phillips-Silver, J., Trainor, L.J., 2008. Vestibular influence on auditory metrical interpretation. Brain Cogn. 67, 94–102.
Picton, T.W. (Ed.), 2011. Human Auditory Evoked Potentials. Plural Publishing, San Diego.
Picton, T.W., Hillyard, S.A., Krausz, H.I., Galambos, R., 1974. Human auditory evoked potentials. I. Evaluation of components. Electroencephalogr. Clin. Neurophysiol. 36, 179–190.
Probst, T., Wist, E.R., 1990. Electrophysiological evidence for visual – vestibular interaction in man. Neurosci. Lett. 108, 255–260.
Rosengren, S.M., Colebatch, J.G., 2006. Vestibular evoked potentials (VsEPs) in patients with severe to profound bilateral hearing loss. Clin. Neurophysiol. 117, 1145–1153.
Rosengren, S.M., Todd, N.P.M., Colebatch, J.G., 2005. Vestibular-evoked extraocular potentials produced by stimulation with bone-conducted sound. Clin. Neurophysiol. 116, 1938–1948.
Roucoux-Hanus, M., Boisacq-Schepens, N., 1977. Ascending vestibular projections – further results at cortical and thalamic levels in cat. Exp. Brain Res. 29, 283–292.
Scherg, M., Vajsar, J., Picton, T.W., 1989. A source analysis of the late human auditory evoked potentials. J. Cog. Neurosci. 1, 336–355.
Schlindwein, P., Mueller, M., Bauermann, T., Brandt, T., Stoeter, P., Dieterich, M., 2008. Cortical representation of saccular vestibular stimulation: VEMPs in fMRI. Neuroimage 39, 19–31.
Smith, A.T., Wall, M.B., Thilo, K.V., 2012. Vestibular inputs to human motion-sensitive visual cortex. Cereb. Cortex 22, 1068–1077.
Sohmer, H., Elidan, J., Plotnik, M., Freeman, S., Sockalingam, R., Berkowitz, Z., Mager, M., 1999. Effect of noise on the vestibular system-vestibular evoked potential studies in rats. Noise Health 2, 41–51.
Stenfelt, S., Hakansson, B., Tjellstrom, A., 2000. Vibration characteristics of bone conducted sound *in vitro*. J. Acoust. Soc. Am. 107, 422–431.
Suzuki, M., Kitano, H., Ito, R., Kitanishi, T., Yazawa, Y., Ogawa, T., Shiino, A., Kitajima, K., 2001. Cortical and subcortical vestibular response to caloric stimulation detected by functional magnetic resonance imaging. Cogn. Brain Res. 12, 441–449.
Tait, J., 1932. Is all hearing cochlear? Ann. Otol. Rhinol. Laryngol. 41, 6812.
Thornton, A.R., Mendel, M.I., Anderson, C.V., 1977. Effects of stimulus frequency and intensity on the middle components of the averaged auditory electroencephalic response. J. Speech Lang. Hear. Res. 20, 81–94.
Todd, N.P.M., 2001. Evidence for a behavioral significance of saccular acoustic sensitivity in humans. J. Acoust. Soc. Am. 110, 380–390.
Todd, N.P.M., 2007. Estimated source intensity and active space of the American alligator (*Alligator Mississippiensis*) vocal display. J. Acoust. Soc. Am. 122, 2906–2915.
Todd, N.P.M., Cody, F.W., 2000. Vestibular responses to loud dance music: a physiological basis of the "rock and roll threshold". J. Acoust. Soc. Am. 107, 496–500.
Todd, N.P.M., Merker, B., 2004. Siamang gibbons exceed the saccular threshold: intensity of the song of Hylobates syndactylus. J. Acoust. Soc. Am. 115, 3077–3080.
Todd, N.P.M., 1993. Vestibular feedback in musical performance – response to somatosensory feedback in musical performance. Mus. Percept. 10, 379–382.
Todd, N.P.M., Rosengren, S.M., Aw, S.T., Colebatch, J.G., 2007. Ocular vestibular evoked myogenic potentials (OVEMPs) produced by air- and bone-conducted sound. Clin. Neurophysiol. 118, 381–390.
Todd, N.P.M., Rosengren, S.M., Colebatch, J.G., 2003. A short latency vestibular evoked potential (VsEP) produced by bone-conducted acoustic stimulation. J. Acoust. Soc. Am. 114, 3264–3272.
Todd, N.P.M., Rosengren, S.M., Colebatch, J.G., 2008a. A source analysis of short-latency vestibular evoked potentials produced by air- and bone-conducted sound. Clin. Neurophysiol. 119, 1881–1894.
Todd, N.P.M., Rosengren, S.M., Colebatch, J.G., 2008b. Tuning and sensitivity of the human vestibular system to low-frequency vibration. Neurosci. Lett. 444, 36–41.
Todd, N.P.M., Rosengren, S.M., Colebatch, J.G., 2009. A utricular origin of frequency tuning to low-frequency vibration in the human vestibular system? Neurosci. Lett. 451, 175–180.
Todd, N.P.M., Rosengren, S.M., Govender, S., Colebatch, J.G., 2010. Single trial detection of human vestibular evoked myogenic potentials is determined by signal to noise ratio. J. Appl. Physiol. 109, 53–59.
Wang, Y.-P., Young, Y.-H., 2007. Vestibular-evoked myogenic potentials in chronic noise-induced hearing loss. Otolaryngol. Head Neck Surg. 137, 607–611.
Young, E.D., Fernandez, C., Goldberg, J.M., 1977. Responses of squirrel-monkey vestibular neurones to audio-frequency sound and head vibration. Acta Oto-Laryngol. 84, 352–360.
Zhang, A.S., Govender, S., Colebatch, J.G., 2011. Tuning of the ocular vestibular evoked myogenic potential (oVEMP) to AC sound shows two separate peaks. Exp. Brain Res. 213, 111–116.
Zhang, A.S., Govender, S., Colebatch, J.G., 2012. Tuning of the ocular vestibular evoked myogenic potential to bone-conducted sound stimulation. J. Appl. Physiol. 112, 1279–1290.
Zuniga, M.G., Dinkes, R.E., Davalos-Bichara, M., Carey, J.P., Schubert, M.C., King, W.M., Walston, J., Agrawal, Y., 2012. Association between hearing loss and saccular dysfunction in older individuals. Otol. Neurotol. 33, 1586–1592.